# Impacts of Free-Tropospheric Temperature and Humidity on Nocturnal Nonprecipitating Marine Stratocumulus

XUKUN XU AND HUIWEN XUE

*Department of Atmospheric and Oceanic Sciences, School of Physics, Peking University, Beijing, China*

(Manuscript received 20 December 2014, in final form 16 April 2015)

ABSTRACT

Marine stratocumulus (MSc) cloud amount can decrease with an increase in the cloud-top instability parameter $\kappa$, based on the cloud-top entrainment instability (CTEI) theory. Notice that if boundary layer temperature and humidity remain the same, a given $\kappa$ can correspond to different combinations of free-tropospheric temperature and humidity. By employing large-eddy simulations coupled with bin microphysics, this study investigates the characteristics of three nocturnal nonprecipitating MSc systems with the same $\kappa$ but different free-tropospheric conditions. It is found that the spread of liquid water path (LWP) among the three cases is large. The LWPs of these three cases are also compared with the base case where $\kappa$ is smaller. One of the three cases even has larger LWP than the base case, which is not expected by the CTEI theory. Results indicate that the thermodynamic properties of the free-tropospheric air are important. For the three cases with the same $\kappa$, cooler and moister free-tropospheric air leads to a cooler and moister boundary layer through entrainment, hence a lower cloud base. A cooler and moister free troposphere also allows the turbulent boundary layer air parcels to overshoot to a higher height, leading to a higher cloud top. Therefore, there is a spread in LWPs among systems with the same $\kappa$. The spread can be so large that sometimes systems with larger $\kappa$ may have larger LWPs than systems with smaller $\kappa$. More simulations are also performed covering other free tropospheric conditions and aerosol concentrations.

## 1. Introduction

Covering one-fifth of the world's oceans and greatly raising Earth's albedo (Hartmann et al. 1992; Hahn and Warren 2007), marine stratocumulus (MSc) plays a critical role in controlling Earth's climate. It has been estimated that a 5% increase in the global MSc cloud coverage would be sufficient to offset the global warming induced by the doubling of $CO_2$ (Randall et al. 1984; Slingo 1990). Besides, many of the uncertainties in current climate model can be attributed to our inadequate knowledge of the MSc (Stocker et al. 2014).

Some of the most favored places for MSc clouds are in the eastern parts of subtropical oceans where the subsidence branches of Walker and Hadley circulations locate. Warm and dry free-tropospheric air in these areas serves as a lid for the MSc clouds growing in the cold and moist boundary layer. MSc clouds in these areas are often homogeneous in space and persistent in time.

Thermodynamic properties of the free troposphere would exert significant impacts on MSc. Early study on the impacts of the free troposphere can date back to the cloud-top entrainment instability (CTEI) theory (Lilly 1968; Randall 1980; Deardorff 1980). The theory suggests that when the cloudy air mixes with the entrained free-tropospheric air, it can go through evaporative cooling, become negatively buoyant, and sink away from the cloud top (Randall 1980; Deardorff 1980). When it happens, this is believed to enhance the cloud-top entrainment and trigger a positive feedback, causing the cloud to break up. The researches about CTEI lead to the findings of the cloud-top entrainment instability parameter:

$$\kappa = 1 + \frac{\Delta\theta_l}{\left(\frac{L}{C_p}\right)\Delta q_t}. \tag{1}$$

In Eq. (1), $\theta_l$ is the liquid water potential temperature, $q_t$ is the total water mixing ratio, $L$ is the latent heat of vaporization of water, $C_p$ is the specific heat capacity of dry

*Corresponding author address:* Huiwen Xue, Department of Atmospheric and Oceanic Sciences, School of Physics, Peking University, Room 518, North Physics Building, 209 Chengfu Road, Beijing 100871, China.
E-mail: hxue@pku.edu.cn

DOI: 10.1175/JAS-D-14-0387.1

air, and $\Delta x$ is the difference of $x$ between the layer just above and just below the inversion. Notice that the free troposphere is usually warmer and drier than the boundary layer, so $\Delta\theta_l$ is positive while $\Delta q_t$ is negative. Larger $\kappa$ corresponds to larger cloud-top entrainment instability, which is thought to be easier for the cloud to break up. When thermodynamic properties in the boundary layer remain the same, the value of $\kappa$ is determined by the free-tropospheric conditions: smaller free-tropospheric $\theta_l$ (i.e., smaller $\Delta\theta_l$) and/or smaller free-tropospheric $q_t$ (i.e., larger $|\Delta q_t|$) means a larger $\kappa$. Besides, much smaller free-tropospheric $\theta_l$ and larger free-tropospheric $q_t$ (i.e., much smaller $\Delta\theta_l$ with smaller $|\Delta q_t|$) leads to a larger $\kappa$, too.

It is initially thought that stable stratocumulus can exist only when $\kappa$ is less than a specific criterion (e.g., $\kappa < 0.23$; Kuo and Schubert 1988). However, both field measurements and laboratory experiments later provide evidences that stable MSc clouds exist even when $\kappa$ is larger than 0.23 (e.g., MacVean and Mason 1990; Siems et al. 1990; Duynkerke 1993; Lilly 2002). This is partly because processes such as surface latent heat flux and cloud-top radiative cooling may dominate over the cloud-dessicating effects of CTEI (Yamaguchi and Randall 2008) and therefore CTEI may not be a sufficient condition for the breakup of stratocumulus layers (Stevens et al. 2003a; Mellado et al. 2014).

Nevertheless, $\kappa$ is still useful in understanding stratocumulus (Wood 2012). Recent studies suggest that other things being equal, some of the properties of MSc clouds can be closely related to $\kappa$ when $\kappa$ is in certain range (Moeng 2000; Lock 2009; Noda et al. 2013; van der Dussen et al. 2014). For instance, Lock (2009) found the stratocumulus sheet cover in stratified boundary layer decreases smoothly as $\kappa$ increases (from ~0.2 to ~0.5) while Noda et al. (2013) revealed a nearly linear relationship between decreasing LWP and increasing $\kappa$ in the transient range (with $0.2 < \kappa < 0.6$). Given that there are also studies researching the impacts of free-tropospheric humidity and temperature, respectively (e.g., Ackerman et al. 2004; Chen et al. 2011; Petters et al. 2013), it would be interesting to see if the $\kappa$ parameter could truly represent the impacts of both free-tropospheric humidity and temperature collectively.

Considering that one $\kappa$ might correspond to different sets of free-tropospheric humidity and temperature, the first step to see if $\kappa$ will serve as a good parameter is to investigate the spread of cloud properties among MSc systems with the same $\kappa$ but different free troposphere. If the spread of the cloud properties among the same $\kappa$ cases is small, it would be reasonable to connect the MSc cloud properties with $\kappa$ as we used to; if the spread of the cloud properties among the same $\kappa$ cases is large, it would invite new insights on the impacts of free troposphere. Also notice that as some general circulation models are based on an empirical relationship to diagnose MSc cloud amount using the thermodynamic jumps (e.g., Klein and Hartmann 1993; Wood and Bretherton 2006; van der Dussen et al. 2014), the analysis of how the MSc cloud amounts are influenced by the free-tropospheric thermodynamic properties (with boundary layer properties remain the same) may add insight to the parameterization of MSc clouds in larger-scale models as well.

By employing a large-eddy model coupled with bin microphysics, this study tries to reveal the complexity of the impact of free-tropospheric thermodynamic properties on MSc. Starting from a base case, three MSc cases with a same $\kappa$ are simulated and analyzed. We then expand our simulations to other meteorological conditions. Since cloud drop size and number greatly affect the cloud-top evaporative cooling, which plays an important role in cloud-top entrainment (Sandu et al. 2008; Caldwell and Bretherton 2009; Lu et al. 2013), sensitivity tests with regard to the aerosol concentration are conducted by repeating our experiments over an aerosol concentration range from 50 to 500 $\mathrm{mg}^{-1}$. Sensitivity of our results to domain size is also considered. Discussion will be provided in section 4, followed by the conclusion in section 5.

## 2. Method

### a. Large-eddy model

The tool used in this study is the UCLA-LES model (Stevens et al. 1999) coupled with a bin microphysics scheme [Tzivion (Tzitzvashvili) et al. 1987; Feingold et al. 1996; Stevens et al. 1996]. Details of the scheme are given by Xue and Feingold (2006). In the bin microphysics scheme, 25 bins are used, covering a radius range of approximately 1.5–1000 $\mu$m. Only warm cloud microphysical processes are considered in the scheme with assumptions on the aerosol size distribution (lognormal, with median radius $r_g = 0.1$ $\mu$m and geometric standard deviation $\sigma_g = 1.5$) and composition (full-soluble ammonium sulfate). A longwave radiative forcing parameterization derived from delta-four stream model (Fu and Liou 1993) is adopted as described in Stevens et al. (2005). No shortwave radiation scheme has been employed as we focus on the nocturnal MSc.

### b. Case description and experimental setup

The initial setups are based on the second Dynamics and Chemistry of the Marine Stratocumulus (DYCOMS-II) research flight 1 (RF01) (Stevens et al. 2003b, 2005). The cloud remains an ideal stratocumulus deck both spatially and temporally (Stevens et al. 2003b) and without detectable drizzle (vanZanten et al. 2005).

TABLE 1. Free-tropospheric settings of experiments.

| Exp | $\theta_{lf}$ ($\Delta\theta_l$) (K) | $q_{tf}$ ($\lvert\Delta q_t\rvert$) (g kg$^{-1}$) | $\kappa$ |
|---|---|---|---|
| Base | 298.0 (9.0) | 1.5 (7.5) | 0.51 |
| KpT | 296.5 (7.5) | 1.5 (7.5) | 0.59 |
| KpQ | 298.0 (9.0) | 0.0 (9.0) | 0.59 |
| KpTQ | 295.0 (6.0) | 3.0 (6.0) | 0.59 |

Thermodynamic parameters used in the model are tuned to be the same as in Stevens et al. (2005).

The initial profiles of liquid water potential temperature $\theta_l$ and total water mixing ratio $q_t$ for this study are

$$\theta_l = \begin{cases} 289.0\,\mathrm{K} & z \le z_i \\ \theta_{lf} + (z - z_i)^{1/3}\,\mathrm{K} & z > z_i \end{cases} \quad \text{and} \tag{2}$$

$$q_t = \begin{cases} 9.0\,\mathrm{g\,kg^{-1}} & z \le z_i \\ q_{tf}\,\mathrm{g\,kg^{-1}} & z > z_i \end{cases}, \tag{3}$$

with $z$ being the height and $z_i = 840$ m being the inversion height. For our base case, $\theta_{lf} = 298$ K and $q_{tf} = 1.5$ g kg$^{-1}$, which are very close to the settings in Stevens et al. (2005). The subscript $f$ refers to parameters of the free troposphere. The temperature jump $\Delta\theta_l$ is calculated as the difference between $\theta_{lf}$ and $\theta_l$ just below the inversion layer (i.e., 289.0 K). The humidity jump $\Delta q_t$ is calculated in a similar way. The base case has a $\kappa$ of 0.51.

From the base case, we increase the $\kappa$ of the system from 0.51 to 0.59 by keeping the boundary layer conditions the same but changing the properties of the free troposphere in three ways: 1) decreasing $\theta_{lf}$ (KpT case), 2) decreasing $q_{tf}$ (KpQ case), and 3) decreasing $\theta_{lf}$ but increasing $q_{tf}$ (KpTQ case). By varying the meteorological field as big as possible with the same $\kappa$, we aim at exploring how different the cloud properties can be when $\kappa$ are the same. Exact values of $\theta_{lf}$ and $q_{tf}$ in the setups are listed in Table 1 along with the thermodynamic jumps and specific $\kappa$ for each case. Initial profiles of the simulations are plotted in Fig. 1.

After careful analysis for the above cases, we performed another $7 \times 7$ LESs with initial $\theta_{lf}$ from 295 to 298 K with an interval of 0.5 K and $q_{tf}$ from 0 to 3 g kg$^{-1}$ with an interval of 0.5 g kg$^{-1}$, covering the $\kappa$ range from 0.4 to 0.7 approximately. This will provide a more general description of the MSc cloud properties in the above parameter space.

All simulations above are conducted with an aerosol concentration of 100 mg$^{-1}$. Simulations at other aerosol concentrations ($N_a$ = 50, 200, and 500 mg$^{-1}$) are also performed.

A fixed horizontal spacing of $\Delta x = \Delta y = 35$ m and a varied vertical spacing with 10-m resolution near the surface and 5-m resolution in the vicinity of cloud top are adopted as in Stevens et al. (2005). A 2.1 km $\times$ 2.1 km $\times$ 1.5 km domain size is used for computational efficiency. All simulations run for 6 h, with the last 4 h used for analysis. A simulation with a fourfold domain size is conducted as a sensitivity test. No sign of marked impact on the flow statistics is found.

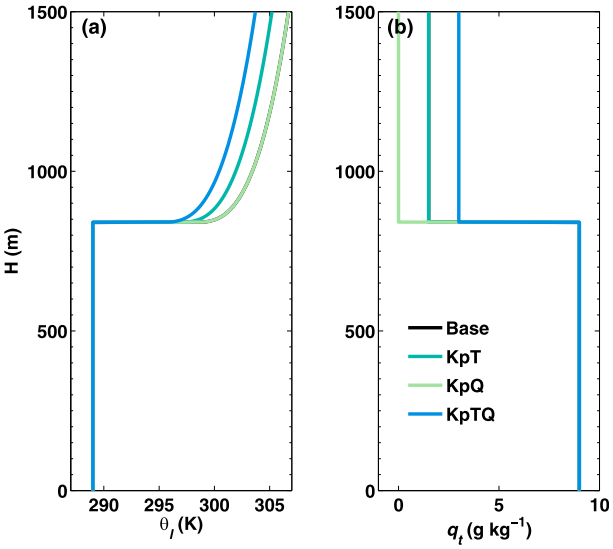


FIG. 1. Initial profiles of experiments: (a) liquid water potential temperature and (b) total water mixing ratio. The inversion height is 840 m. The base case (black) is overlapped by the KpQ case (light green) in (a) and by the KpT case (cyan) in (b).

The cloud-top entrainment rate $w_e$ is computed using the following formula:

$$w_e = \frac{d\overline{z}_i}{dt} - w_s. \tag{4}$$

To derive the average inversion height $\overline{z}_i$, we first compute the local inversion height $z_i$ by locating the maximum gradient in total water mixing ratio along the vertical direction. The heights are then horizontally averaged to get $\overline{z}_i$. The term $w_s$ in Eq. (4) is the large-scale subsidence, defined as

$$w_s = -Dz_i, \tag{5}$$

where $D$ is the horizontal divergence and set to be $3.75 \times 10^{-6}$ s$^{-1}$ in our simulation.

## 3. Results

### a. Overview of the MSc cloud amount

Time series of cloud fraction and domain-averaged LWP at an aerosol concentration of 100 mg$^{-1}$ for the base, KpT, KpQ, and KpTQ cases are shown in Fig. 2. Notice that all cloud fractions are close to 1, while LWPs are quite different among the four cases.

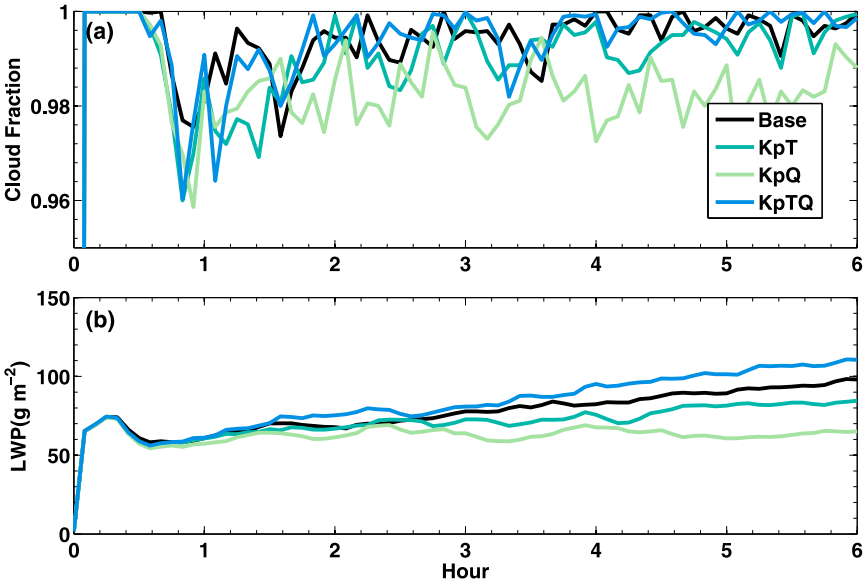


FIG. 2. Time series for the base, KpT, KpQ, and KpTQ cases at an aerosol concentration of 100 mg$^{-1}$: (a) cloud fraction for the four cases and (b) domain-averaged LWP for the four cases.

LWP of the base case is similar to that of Ackerman et al. (2004), where a bin microphysics scheme is adopted, and is consistent with the observation (Stevens et al. 2003b). Compared to the base case, both the KpT and KpQ cases have lower LWPs as seen in Fig. 2b. This is expected from former studies, because the KpT and KpQ cases have larger $\kappa$ so that clouds suffer more from the desiccating effects of the enhanced entrainment of the free-tropospheric air.

On the other hand, although the increase in $\kappa$ (from 0.51 to 0.59) is the same for both cases, their decreases in LWPs are different. The decrease in LWP in the KpQ case is about 2 times larger than that of the KpT case near the end of the simulation (Fig. 2b). The KpTQ case even has higher LWP than the base case (Fig. 2b), although its $\kappa$ is larger. The cloud in the KpTQ case seems not being desiccated by the entrained free-tropospheric air as much as in the KpT or KpQ case.

Given that the KpT, KpQ, and KpTQ cases all have the same $\kappa$, the spread of LWP among the cases is large. To explain why cases with the same $\kappa$ but different free-tropospheric conditions can be quite different in their LWPs (e.g., KpQ versus KpT case in Fig. 2b), and why larger $\kappa$ sometimes leads to larger LWP (e.g., KpTQ versus base case in Fig. 2b), we have to look at how the boundary layers evolve in these cases.

### b. *Impact on the boundary layer properties*

Figure 3 shows the vertical profiles of liquid water potential temperature $\theta_l$, total water mixing ratio $q_t$, and liquid water content (LWC) averaged in the third hour (first hour after spinup, first row) and sixth hour (last hour of simulation, second row) for the base, KpT, and KpQ cases. In the third hour, thermodynamic and LWC profiles in the boundary layers of all three cases are very similar, with only the temperature of the KpT and KpQ cases being slightly lower than that of the base case, as shown by the nearly overlapped lines in Figs. 3a–c.

However, thermodynamic profiles for the three cases become apparently different in the sixth hour. The boundary layers of the KpT and KpQ cases are warmer and drier than the base case. Table 2 shows the time-averaged entrainment rates $w_e$ for the four cases. Notice that the KpT and KpQ cases have higher entrainment rates than the base case (Table 2). It means more free-tropospheric air, which is warm and dry compared to that of the boundary layer air, is entrained to the boundary layer. Their boundary layers are thus warmer and drier than the base case (see Figs. 3d,e).

Boundary layer properties between the KpT and KpQ cases also differ at the sixth hour, although they have the same $\kappa$ and similar entrainment rate. The KpT case has cooler and moister boundary layer because the KpT case has cooler and moister free-tropospheric air than the KpQ case (Table 1). This result indicates that the thermodynamic properties of the free-tropospheric air have impacts not only on the cloud-top entrainment strength but also the boundary layer properties after the free-tropospheric air is entrained.

Cooler and moister boundary layer leads to lower lifting condensation level and makes the clouds to form at a lower altitude. The base case has the lowest cloud-base

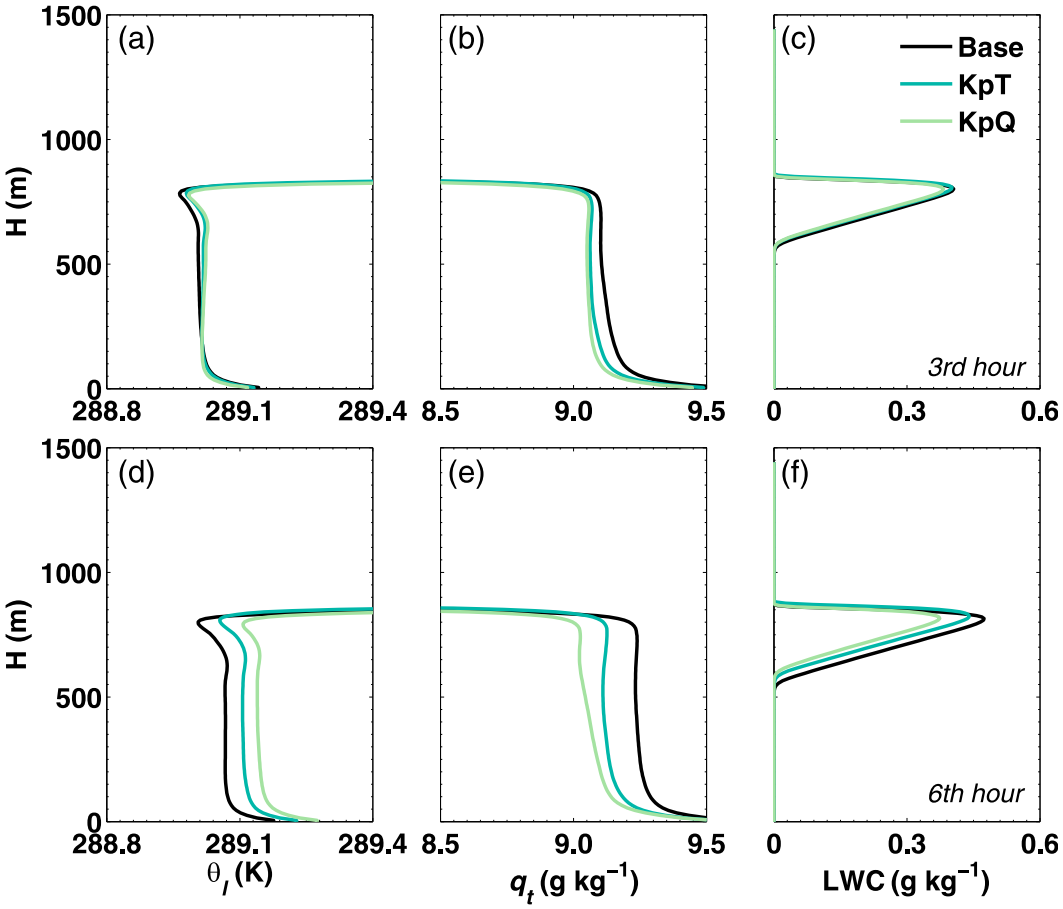


FIG. 3. Vertical profiles in the (a)–(c) third hour (first hour after spinup) and (d)–(f) sixth hour (last hour of simulation) for the base case (black), KpT case (cyan), and KpQ case (light green): (a),(d) total water mixing ratio, (b),(e) liquid water potential temperature, and (c),(f) liquid water content.

height because the least free-tropospheric air is entrained. The cloud-base height of the KpT case is lower than that of the KpQ case because the entrained free troposphere is cooler and moister, as seen in Fig. 3f.

### c. *Impact on the boundary layer height*

Figure 4 shows the same plot as Fig. 3 but for the base case and the KpTQ case. Again, in the third hour, the thermodynamic and LWC profiles in the boundary layers are almost identical. As the simulation goes, more air is entrained into the boundary layer in the KpTQ case (Table 2). However, the cooler and moister nature of the free-tropospheric air in the KpTQ case causes less change to the boundary layer. The net effect at the sixth hour is that the two cases have similar boundary layer thermodynamic properties regardless that the KpTQ case has larger $\kappa$ and a larger entrainment rate (Figs. 4a–c).

Notice that the cloud top in the KpTQ case is higher than that of the base case (Fig. 4f). Explanations of this are possible by analyzing how easily an air parcel in the boundary layer would overshoot to the free troposphere. Because of the turbulent nature of the boundary layer, there are always overshooting air parcels impinging though the inversion layer. In a cooler free troposphere (but still much warmer than the boundary layer), the air above the inversion layer is denser. The overshooting air parcels would experience less negative buoyant force and thus stop at a higher height. In a moister free troposphere (but still much drier than the boundary layer), cloud water evaporation is slower. The

TABLE 2. Cloud-top entrainment rate $w_e$ averaged over the last 4 h.

| Exp | $w_e$ (cm s$^{-1}$) |
|---|---|
| Base | 0.46 |
| KpT | 0.53 |
| KpQ | 0.51 |
| KpTQ | 0.61 |

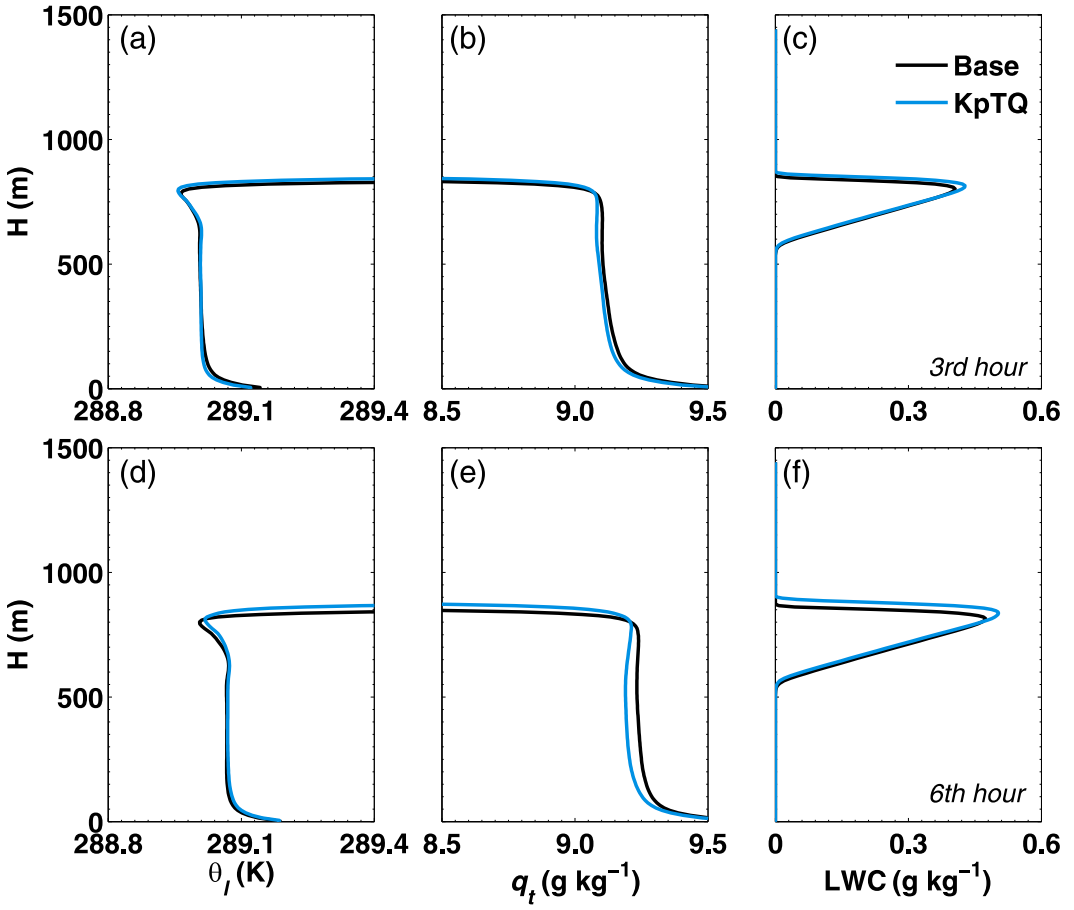


FIG. 4. As in Fig. 3, but for the base case (black) and KpTQ case (blue).

overshooting air parcels would experience less evaporative cooling and thus stop at a higher height. Therefore, in the case of both cooler and moister free troposphere as in the KpTQ case, the cloud top is higher. As the boundary layer grows, the air parcels now overshoot at higher altitudes, pushing the inversion layer even higher (Figs. 4d–e).

In fact, such phenomenon has been addressed by Randall (1984) theoretically. Randall predicted that under certain conditions, cloud-top entrainment will build the cloud rather than destroy it by lifting the cloud-top height more than the cloud-base height. The so-called cloud deepening through entrainment (CDE) effect proposed by Randall (1984) is confirmed in this study by the large-eddy simulations.

### *d. Comprehensive results of free-tropospheric impacts*

Apparently, the LWP of the near-adiabatic MSc cloud in our study depends on both cloud-base height and cloud-top height: for cases with the same $\kappa$, the cooler and moister the free-tropospheric air, the cooler and moister the boundary layer and the lower the cloud base. At the same time, a cooler and moister free troposphere makes upward motion of the air parcels more easily, so the cloud top will also be higher. Therefore, there would be a large spread in LWPs among MSc with the same $\kappa$. For cases with the same $\kappa$, the ones with a cooler and moister free troposphere tend to have larger LWPs.

With all the complicated processes discussed above, it is helpful to have a general picture of how the MSc clouds behave under different free-tropospheric conditions. Figure 5 shows the time- and domain-averaged LWP as a function of free-tropospheric temperature and humidity. Different $\kappa$ are indicated by the white dashed lines. The initial boundary layers are set exactly the same as the former cases discussed above.

Consistent with previous studies, when the $\kappa$ is larger (i.e., free troposphere is cooler and/or drier), the inversion layer is more unstable. The LWP of MSc is generally smaller as well. As $\kappa$ changes from 0.4 to 0.7, LWP can change from about 100 to 50 g m$^{-2}$. However, aside from the stability of the inversion layer, both the thermodynamic properties of the entrained air and the height of the inversion layer also play roles in deciding

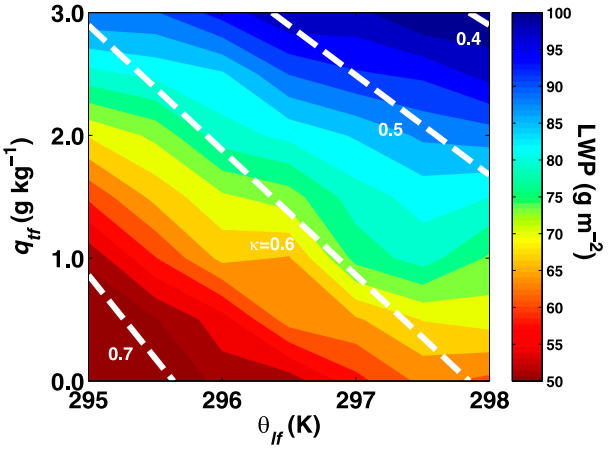


FIG. 5. Time- and domain-averaged LWP for the 7 × 7 LESs with initial $\theta_{lf}$ from 295 to 298 K with an interval of 0.5 K and $q_{tf}$ from 0 to 3 g kg$^{-1}$ with an interval of 0.5 g kg$^{-1}$. Each white dashed line indicates $\kappa$ of the same value. Notice that LWP varies greatly along the each $\kappa$ line.

the LWP. As shown in Fig. 5, the constant $\kappa$ lines are not parallel with the constant LWP lines. For cases with the same $\kappa$, the spread of the LWP can be rather large. Along each $\kappa$ line, the cooler and moister the free troposphere is, the larger the LWP is. This might shed light on new parameterizations for stratus clouds in larger-scale models. Clearly, more work is needed to quantitatively understand the comprehensive impacts of the free troposphere.

## 4. Discussion

### a. Results at other aerosol concentrations

To examine the possible influences of the aerosol concentration on our results, we repeat experiments over aerosol concentrations of 50, 100, 200, and 500 mg$^{-1}$. The results are shown in Fig. 6. Each point in Fig. 6 represents the time- and domain-averaged LWP of the last 4 h of a simulation at a specific aerosol concentration. It suggests that, for all aerosol concentrations, the spread in LWP among cases with the same $\kappa$ can be quite large. Systems with larger $\kappa$ generally have smaller LWPs but sometimes also larger LWPs.

### b. Potential change in $\kappa$ during simulations

Each of our simulations started at a well-defined $\kappa$, as shown in Table 1. However, as the simulations go on, $\kappa$ is not as clear as before to diagnose. The difficulties come from two parts. On one hand, the definition of the inversion layer is now ambiguous. For instance, the inversion layer can either be defined as the height of the cloud top, or maximum gradient of the sounding, or where turbulent motion become quiet (Moeng et al. 2005). Using different methods to diagnose the inversion layer typically end up with tens of meters of differences in inversion height, which affects the calculation of $\kappa$. On the other hand, the once-sharp thermodynamic transitions near the inversion layer now become ambiguous. Using thermodynamic values in adjacent grids just above and below the inversion layer to calculate $\kappa$ as at the beginning of the simulation would not work for the later hours of the simulations.

Despite the above difficulties, it is found that $\kappa$ do not change much in our simulations. Since $\kappa$ is determined by the structure of the thermodynamic profiles, Fig. 7 is plotted to compare the structure of the profiles at the third hour (first hour after spinup) and the sixth hour (last hour of simulation). As indicated in Fig. 7, the changes in the thermodynamic structures of our simulations are negligible compared to the differences between cases. Therefore, $\kappa$ of each case should stay nearly the same. In addition, we also apply one of the several ways to calculate $\kappa$ numerically in the later hours of the simulation in appendix B. The results there indicate as well that $\kappa$ of the KpT, KpQ, and KpTQ cases remain nearly the same and are larger than that of the base case throughout the simulation.

### c. Sensitivity to domain size

A relative small domain size was adopted in our study for computational efficiency. We therefore test the sensitivity of our results to domain size in simulations with a fourfold domain size. The new simulation has a domain size of 4.2 km × 4.2 km × 1.5 km, all else being the same. Figure 8 shows the buoyancy production, variance of vertical velocity $w$, and time series of domain-averaged LWP and TKE of the base case and the larger-domain case. The thermodynamic properties for the two cases are nearly the same, which indicates the findings in this study are not sensitive to the domain size.

In addition, simulations with a 36-fold domain size (12.6 km × 12.6 km) and bulk microphysics have been performed to better represent the potential effects of cloud structures and circulation patterns. The results are consistent with the findings in Fig. 2 as well (see appendix A).

## 5. Conclusions

This study focuses on the impact of free-tropospheric temperature and humidity on MSc. Inspired by former studies on CTEI, this study investigates how MSc systems behave with the same $\kappa$ but different free-tropospheric conditions. Our results show that even with the same $\kappa$, the LWPs of MSc are quite different. The spread of LWP can be so large that under some conditions,

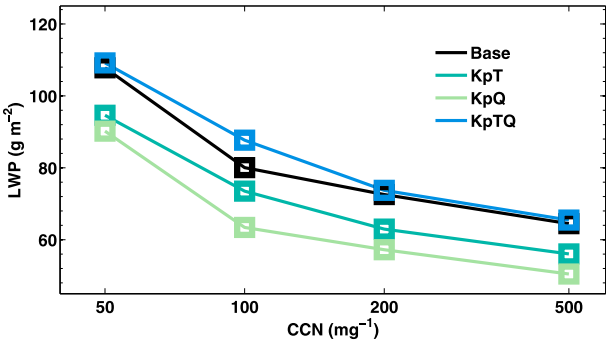


FIG. 6. Time- and domain-averaged LWP during the last 4 h of simulation at aerosol concentrations of 50, 100, 200, and 500 mg$^{-1}$. Notice that the spread of LWP among the same $\kappa$ cases (KpT, KpQ, and KpTQ) is persistent at various aerosol concentrations in this study.

cases with larger $\kappa$ could have larger LWPs than cases with smaller $\kappa$. This is not expected by the CTEI theory, where it is proposed that clouds with larger $\kappa$ would dissipate more easily.

Results show that the entrained free-tropospheric air will gradually change the thermodynamic properties of the boundary layer through turbulent mixing. The impacts of the free-tropospheric air on boundary layer clouds depend not only on $\kappa$ and entrainment rate, but also on the properties of the entrained air. For cases with the same $\kappa$, the case with cooler and moister free troposphere will end up with a cooler and moister boundary layer. The cooler and moister boundary layer makes it easier for water to condensate, so the cloud base is lower.

The properties of the free-tropospheric air also affect cloud-top height. Boundary layer air parcels tend to behave differently when they overshoot into a cooler and moister versus a warmer and drier free troposphere. The overshooting air parcels, which are believed to be responsible for the boundary layer growth, would experience less resistance in a cooler and moister free troposphere. When the free troposphere is cool and moist enough, the overshooting process is strong and the growth of the boundary layer will be fast enough to overcome the large-scale subsidence, leading to a higher cloud top. The CDE hypothesis proposed by Randall (1984) is confirmed in this study.

In the end, we further expand our experiments to other meteorological settings and aerosol concentrations. The findings are generally the same. For cases with the same $\kappa$, the spread of LWP is large. Sensitivity test of the simulation to the domain size has also been conducted and passed, although the simulation with a fourfold domain size still lacks the ability to incorporate any effects of the mesoscale circulation.

It should be noted that stratocumulus systems with the same $\kappa$ could have different LWP owing to the differences in latent heat flux, large-scale subsidence, shortwave heating, and whether the systems are precipitating or nonprecipitating and coupled or noncoupled (e.g., van der Dussen et al. 2014; Xiao et al. 2011; Yamaguchi and Randall 2008). However, the fact that stratocumulus systems with the same $\kappa$ often have different free-tropospheric conditions is often ignored. This study shows that different free-tropospheric conditions exert

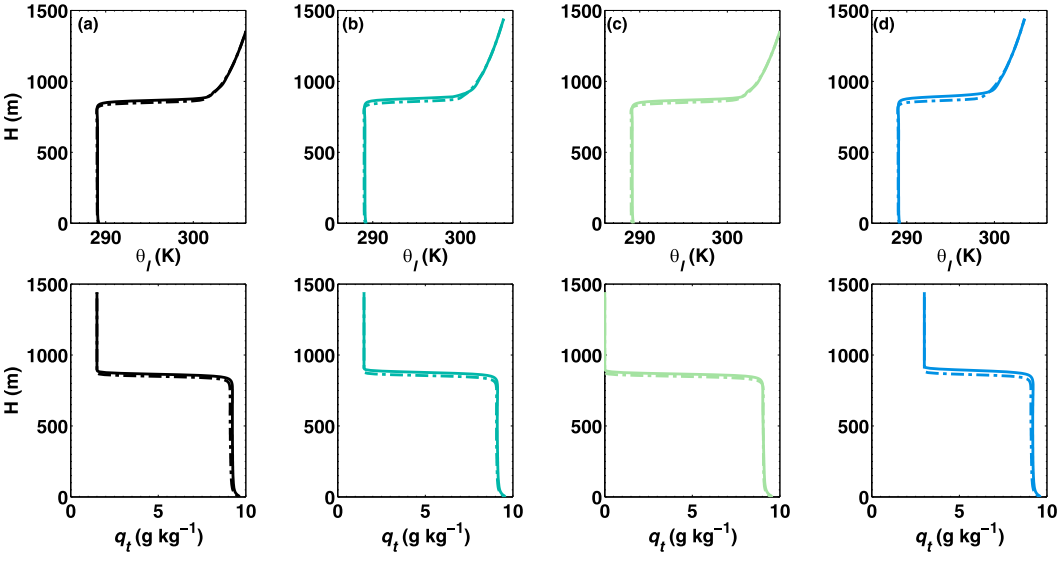


FIG. 7. $\theta_l$ and $q_t$ profiles for (a) base, (b) KpT, (c) KpQ, and (d) KpTQ cases. Dashed–dotted lines stand for profiles at the third hour (first hour after spinup) and the solid lines stand for profiles at the sixth hour (last hour of simulation). Notice that the structures of the thermodynamic profiles nearly do not change throughout the simulation.

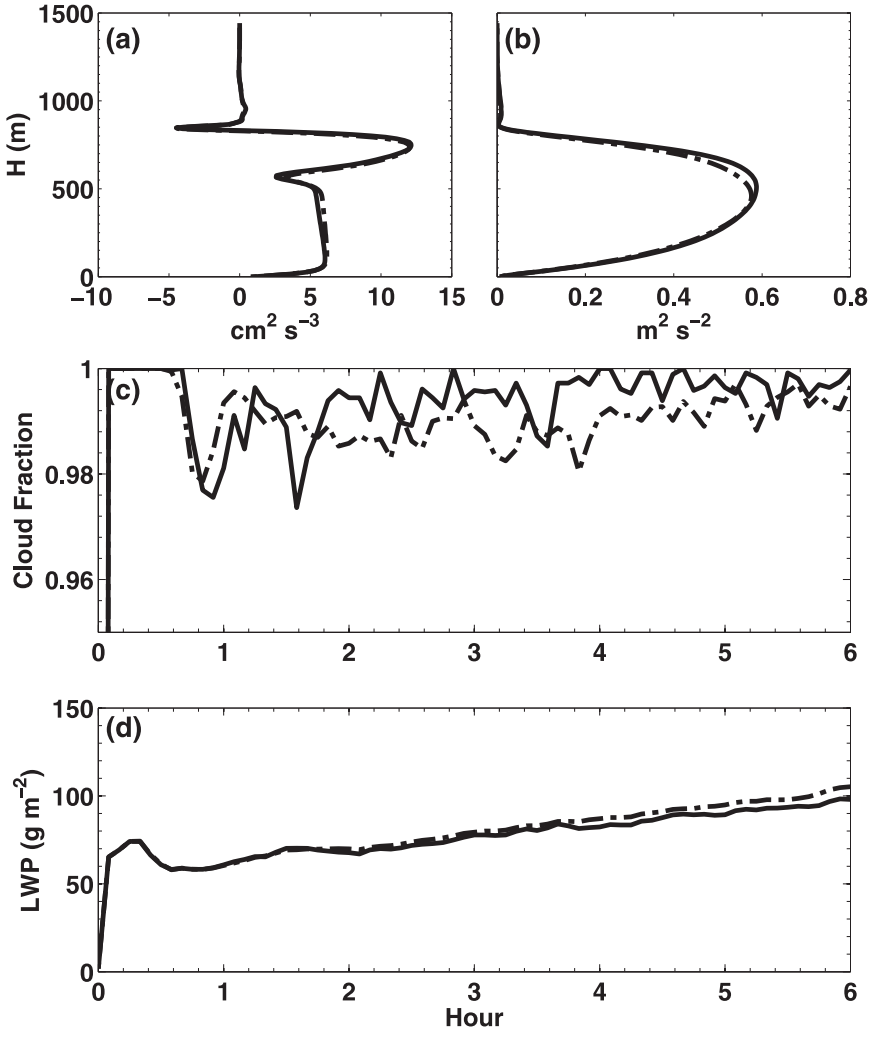


FIG. 8. Time- and domain-averaged vertical profiles during the last 4 h of simulation: (a) revolved buoyancy production and (b) variance of vertical velocity $w$. Time series of (c) cloud fraction and (d) domain-averaged LWP. Solid lines stand for the base case and dashed–dotted lines stand for the larger-domain case.

different impacts on the LWP of stratocumulus systems as well.

This study also indicates that both temperature jump $\Delta\theta_l$ and humidity jump $\Delta q_t$ may play roles in determining the properties of MSc and both should be considered in MSc parameterization for larger models. However, future work is needed to account for the potential correlations between free-tropospheric temperature and humidity, and the relations between these thermodynamic properties and large-scale subsidence.

*Acknowledgments.* This project is supported by Chinese NSF Grant 41275144 and Chinese 973 program under Grant 2013CB955803. We thank Prof. Bjorn Stevens for generously providing the LES code. Comments by Dr. Takanobu Yamaguchi, Dr. Chunsong Lu, and Prof. Szymon P. Malinowski are gratefully acknowledged. Discussion with Prof. Robert Wood and Dr. Stephan de Roode is also greatly appreciated.

## APPENDIX A

### Simulations with Large Domain Size and Bulk Microphysics

Simulations with a 36-fold domain size (12.6 km × 12.6 km) and bulk microphysics have been performed to better represent the potential effects of cloud structures and circulation patterns. The results are presented in Fig. A1. The base case results in this study are well

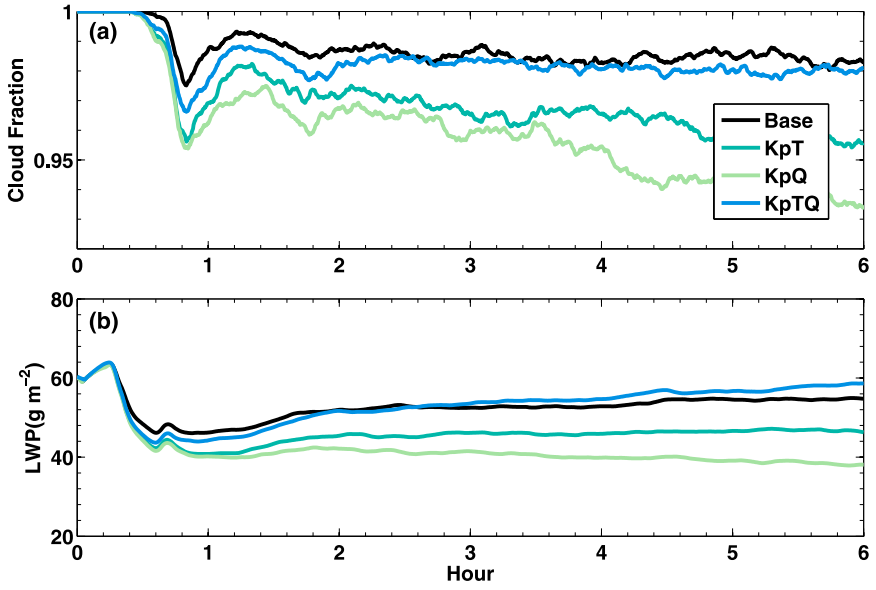


FIG. A1. As in Fig. 2, except that a 12.6 km × 12.6 km × 1.5 km domain size and bulk microphysics are adopted.

within the central half of the ensemble distribution in Stevens et al. (2005, their Fig. 2). The spread in LWP among the KpT, KpQ, and KpTQ cases is obvious. The results are consistent with the findings in the main text.

## APPENDIX B

### Calculating Kappa in the Later Hours of the Simulation

The simulations begin with an idealized inversion layer. The temperature/humidity jumps and thus $\kappa$ are well defined at the beginning. However, in the late hours of the simulations, the inversion layer becomes ambiguous. The temperature/humidity jumps now happen in the entrainment interface layer with a finite thickness (Garratt 1994). Identifying the upper and lower boundary of the entrainment interface layer ($z_+$ and $z_-$) would then be the first step in calculating the temperature/humidity jumps and $\kappa$.

To the best of our knowledge, there is no widely accepted method to locate $z_+$ and $z_-$ yet. Nevertheless, the method in Yamaguchi et al. (2011) is adopted. The $z_+$ and $z_-$ are identified in Yamaguchi et al. (2011) using the variance of liquid water static energy $s_l$:

$$\begin{cases} z_+ = z & \text{at} \quad 0.05\max(\overline{s_l'^2}) \quad \text{above} \quad z_{\max} \\ z_- = z & \text{at} \quad 0.05\max(\overline{s_l'^2}) \quad \text{below} \quad z_{\max} \end{cases},$$

where

$$z_{\max} = z \quad \text{at} \quad \max(\overline{s_l'^2}).$$

We employ this method at each time instant of our output to calculate $\Delta\theta_l$, $\Delta q_t$, and $\kappa$ consistently. The time series of $\kappa$ are presented in Fig. B1. The mean and standard deviation of $\kappa$ for the last 4 h are calculated and shown in Table B1. The results confirm that there is little change in $\kappa$ throughout the simulations. The values of $\kappa$ in the KpT, KpQ, and KpTQ cases remain nearly the same and are larger than that of the base case.

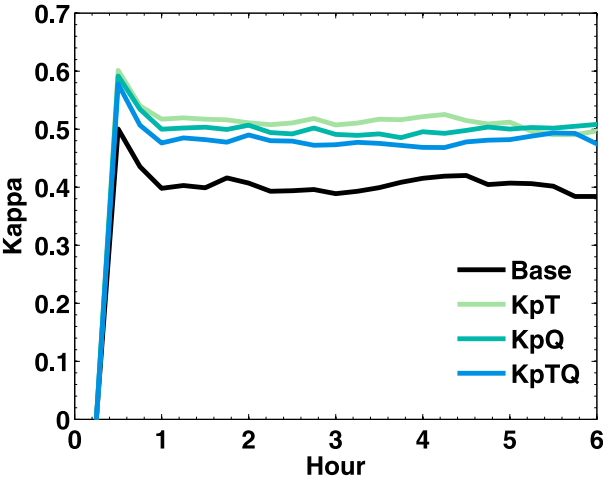


FIG. B1. Time series of $\kappa$ for the base, KpT, KpQ, and KpTQ cases. Notice that the $\kappa$ of the KpT, KpQ, and KpTQ cases remain nearly the same and are larger than that of the base case throughout the simulation.

TABLE B1. Mean and standard deviation of $\kappa$ for the last 4 h.

| Exp | $\overline{\kappa}$ | $\sigma_\kappa$ |
|---|---|---|
| Base | 0.40 | 0.01 |
| KpT | 0.51 | 0.01 |
| KpQ | 0.50 | 0.01 |
| KpTQ | 0.48 | 0.01 |

Notice that the $\kappa$ shown in Table B1 are not exactly the same as the $\kappa$ shown in Table 1, because the method used to calculate $\kappa$ are different. To the best of our knowledge, there is no single method to calculate $\kappa$ for both the beginning and the later hours of the simulations. To better compare with previous studies (e.g., Noda et al. 2013; Lock 2009), only the $\kappa$ at the beginning of the simulations are shown in the main text.

## REFERENCES


Ackerman, A. S., M. P. Kirkpatrick, D. E. Stevens, and O. B. Toon, 2004: The impact of humidity above stratiform clouds on indirect aerosol climate forcing. *Nature,* **432,** 1014–1017, doi:10.1038/nature03174.

Caldwell, P., and C. S. Bretherton, 2009: Response of a subtropical stratocumulus-capped mixed layer to climate and aerosol changes. *J. Climate,* **22,** 20–38, doi:10.1175/2008JCLI1967.1.

Chen, Y.-C., L. Xue, Z. J. Lebo, H. Wang, R. M. Rasmussen, and J. H. Seinfeld, 2011: A comprehensive numerical study of aerosol-cloud-precipitation interactions in marine stratocumulus. *Atmos. Chem. Phys.,* **11,** 9749–9769, doi:10.5194/acp-11-9749-2011.

Deardorff, J. W., 1980: Cloud top entrainment instability. *J. Atmos. Sci.,* **37,** 131–147, doi:10.1175/1520-0469(1980)037<0131:CTEI>2.0.CO;2.

Duynkerke, P. G., 1993: The stability of cloud top with regard to entrainment: Amendment of the theory of cloud-top entrainment instability. *J. Atmos. Sci.,* **50,** 495–502, doi:10.1175/1520-0469(1993)050<0495:TSOCTW>2.0.CO;2.

Feingold, G., B. Stevens, W. R. Cotton, and A. S. Frisch, 1996: The relationship between drop in-cloud residence time and drizzle production in numerically simulated stratocumulus clouds. *J. Atmos. Sci.,* **53,** 1108–1122, doi:10.1175/1520-0469(1996)053<1108:TRBDIC>2.0.CO;2.

Fu, Q., and K. N. Liou, 1993: Parameterization of the radiative properties of cirrus clouds. *J. Atmos. Sci.,* **50,** 2008–2025, doi:10.1175/1520-0469(1993)050<2008:POTRPO>2.0.CO;2.

Garratt, J. R., 1994: *The Atmospheric Boundary Layer.* Cambridge University Press, 336 pp.

Hahn, C. J., and S. G. Warren, 2007: A gridded climatology of clouds over land (1971–96) and ocean (1954–97) from surface observations worldwide. Carbon Dioxide Information Analysis Center, Department of Energy, Oak Ridge, TN, digital media. [Available online at http://cdiac.ornl.gov/epubs/ndp/ndp026e/ndp026e.html.]

Hartmann, D. L., M. E. Ockertbell, and M. L. Michelsen, 1992: The effect of cloud type on Earth's energy balance: Global analysis. *J. Climate,* **5,** 1281–1304, doi:10.1175/1520-0442(1992)005<1281:TEOCTO>2.0.CO;2.

Klein, S. A., and D. L. Hartmann, 1993: The seasonal cycle of low stratiform clouds. *J. Climate,* **6,** 1587–1606, doi:10.1175/1520-0442(1993)006<1587:TSCOLS>2.0.CO;2.

Kuo, H.-C., and W. H. Schubert, 1988: Stability of cloud-topped boundary layers. *Quart. J. Roy. Meteor. Soc.,* **114,** 887–916, doi:10.1002/qj.49711448204.

Lilly, D. K., 1968: Models of cloud-topped mixed layers under a strong inversion. *Quart. J. Roy. Meteor. Soc.,* **94,** 292, doi:10.1002/qj.49709440106.

——, 2002: Entrainment into mixed layers. Part II: A new closure. *J. Atmos. Sci.,* **59,** 3353–3361, doi:10.1175/1520-0469(2002)059<3353:EIMLPI>2.0.CO;2.

Lock, A. P., 2009: Factors influencing cloud area at the capping inversion for shallow cumulus clouds. *Quart. J. Roy. Meteor. Soc.,* **135,** 941–952, doi:10.1002/qj.424.

Lu, C. S., Y. G. Liu, S. J. Niu, S. Krueger, and T. Wagner, 2013: Exploring parameterization for turbulent entrainment-mixing processes in clouds. *J. Geophys. Res. Atmos.,* **118,** 185–194, doi:10.1029/2012JD018464.

MacVean, M. K., and P. J. Mason, 1990: Cloud-top entrainment instability through small-scale mixing and its parameterization in numerical models. *J. Atmos. Sci.,* **47,** 1012–1030, doi:10.1175/1520-0469(1990)047<1012:CTEITS>2.0.CO;2.

Mellado, J. P., B. Stevens, and H. Schmidt, 2014: Wind shear and buoyancy reversal at the top of stratocumulus. *J. Atmos. Sci.,* **71,** 1040–1057, doi:10.1175/JAS-D-13-0189.1.

Moeng, C. H., 2000: Entrainment rate, cloud fraction, and liquid water path of PBL stratocumulus clouds. *J. Atmos. Sci.,* **57,** 3627–3643, doi:10.1175/1520-0469(2000)057<3627:ERCFAL>2.0.CO;2.

——, B. Stevens, and P. P. Sullivan, 2005: Where is the interface of the stratocumulus-topped PBL? *J. Atmos. Sci.,* **62,** 2626–2631, doi:10.1175/JAS3470.1.

Noda, A. T., K. Nakamura, T. Iwasaki, and M. Satoh, 2013: A numerical study of a stratocumulus-topped boundary-layer: Relations of decaying clouds with a stability parameter across inversion. *J. Meteor. Soc. Japan,* **91,** 727–746, doi:10.2151/jmsj.2013-601.

Petters, J. L., H. Jiang, G. Feingold, D. L. Rossiter, D. Khelif, L. C. Sloan, and P. Y. Chuang, 2013: A comparative study of the response of modeled non-drizzling stratocumulus to meteorological and aerosol perturbations. *Atmos. Chem. Phys.,* **13,** 2507–2529, doi:10.5194/acp-13-2507-2013.

Randall, D. A., 1980: Conditional instability of the first kind upside-down. *J. Atmos. Sci.,* **37,** 125–130, doi:10.1175/1520-0469(1980)037<0125:CIOTFK>2.0.CO;2.

——, 1984: Stratocumulus cloud deepening through entrainment. *Tellus,* **36A,** 446–457, doi:10.1111/j.1600-0870.1984.tb00261.x.

——, J. A. Coakley, C. W. Fairall, R. A. Kropfli, and D. H. Lenschow, 1984: Outlook for research on subtropical marine stratiform clouds. *Bull. Amer. Meteor. Soc.,* **65,** 1290–1301, doi:10.1175/1520-0477(1984)065<1290:OFROSM>2.0.CO;2.

Sandu, I., J.-L. Brenguier, O. Geoffroy, O. Thouron, and V. Masson, 2008: Aerosol impacts on the diurnal cycle of marine stratocumulus. *J. Atmos. Sci.,* **65,** 2705–2718, doi:10.1175/2008JAS2451.1.

Siems, S. T., C. S. Bretherton, M. B. Baker, S. S. Shy, and R. E. Breidenthal, 1990: Buoyancy reversal and cloud-top entrainment instability. *Quart. J. Roy. Meteor. Soc.,* **116,** 705–739, doi:10.1002/qj.49711649309.

Slingo, A., 1990: Sensitivity of the Earth's radiation budget to changes in low clouds. *Nature,* **343,** 49–51, doi:10.1038/343049a0.

Stevens, B., G. Feingold, W. R. Cotton, and R. L. Walko, 1996: Elements of the microphysical structure of numerically simulated nonprecipitating stratocumulus. *J. Atmos. Sci.,* **53,** 980–1006, doi:10.1175/1520-0469(1996)053<0980:EOTMSO>2.0.CO;2.

——, C.-H. Moeng, and P. P. Sullivan, 1999: Large-eddy simulations of radiatively driven convection: Sensitivities to the representation of small scales. *J. Atmos. Sci.,* **56,** 3963–3984, doi:10.1175/1520-0469(1999)056<3963:LESORD>2.0.CO;2.

——, and Coauthors, 2003a: On entrainment rates in nocturnal marine stratocumulus. *Quart. J. Roy. Meteor. Soc.,* **129,** 3469–3493, doi:10.1256/qj.02.202.

——, and Coauthors, 2003b: Dynamics and chemistry of marine stratocumulus—Dycoms-II. *Bull. Amer. Meteor. Soc.,* **84,** 579–593, doi:10.1175/BAMS-84-5-579.

——, and Coauthors, 2005: Evaluation of large-eddy simulations via observations of nocturnal marine stratocumulus. *Mon. Wea. Rev.,* **133,** 1443–1462, doi:10.1175/MWR2930.1.

Stocker, T. F., and Coauthors, Eds., 2014: *Climate Change 2013: The Physical Science Basis.* Cambridge University Press, 1535 pp.

Tzivion (Tzitzvashvili), S., G. Feingold, and Z. Levin, 1987: An efficient numerical solution to the stochastic collection equation. *J. Atmos. Sci.,* **44,** 3139–3149, doi:10.1175/1520-0469(1987)044<3139:AENSTT>2.0.CO;2.

van der Dussen, J. J., S. R. de Roode, and A. P. Siebesma, 2014: Factors controlling rapid stratocumulus cloud thinning. *J. Atmos. Sci.,* **71,** 655–664, doi:10.1175/JAS-D-13-0114.1.

vanZanten, M. C., B. Stevens, G. Vali, and D. H. Lenschow, 2005: Observations of drizzle in nocturnal marine stratocumulus. *J. Atmos. Sci.,* **62,** 88–106, doi:10.1175/JAS-3355.1.

Wood, R., 2012: Stratocumulus clouds. *Mon. Wea. Rev.,* **140,** 2373–2423, doi:10.1175/MWR-D-11-00121.1.

——, and C. S. Bretherton, 2006: On the relationship between stratiform low cloud cover and lower-tropospheric stability. *J. Climate,* **19,** 6425–6432, doi:10.1175/JCLI3988.1.

Xiao, H., C.-M. Wu, and C. R. Mechoso, 2011: Buoyancy reversal, decoupling and the transition from stratocumulus to shallow cumulus topped marine boundary layers. *Climate Dyn.,* **37,** 971–984, doi:10.1007/s00382-010-0882-3.

Xue, H. W., and G. Feingold, 2006: Large-eddy simulations of trade wind cumuli: Investigation of aerosol indirect effects. *J. Atmos. Sci.,* **63,** 1605–1622, doi:10.1175/JAS3706.1.

Yamaguchi, T., and D. A. Randall, 2008: Large-eddy simulation of evaporatively driven entrainment in cloud-topped mixed layers. *J. Atmos. Sci.,* **65,** 1481–1504, doi:10.1175/2007JAS2438.1.

——, ——, and M. F. Khairoutdinov, 2011: Cloud modeling tests of the ULTIMATE–MACHO scalar advection scheme. *Mon. Wea. Rev.,* **139,** 3248–3264, doi:10.1175/MWR-D-10-05044.1.